

Diffraction Effect on High-Resolution Liquid-Crystal-on-Silicon Devices

Kuan-Hsu FAN CHIANG*, Shu-Hsia CHEN and Shin-Tson WU¹

*Department of Photonics and Institute of Electro-Optical Engineering, National Chiao Tung University,
 1001 Ta Hsueh Road, Hsinchu 300, Taiwan, Republic of China*

¹*College of Optics and Photonics, University of Central Florida, Orlando, Florida 32816, U.S.A.*

(Received October 1, 2004; accepted January 24, 2005; published May 10, 2005)

We extend the beam propagation method to calculate light propagation in reflective liquid crystal displays. The effect of diffraction on the optical performance of high-resolution liquid-crystal-on-silicon devices is investigated. The light efficiencies are simulated with respect to the pixel pitch for the vertically aligned and finger-on-plane modes. Computer simulation results indicate that the effect of diffraction on these devices is significant. [DOI: 10.1143/JJAP.44.3068]

KEYWORDS: liquid-crystal-on-silicon, beam propagation method, Jones matrix method, diffraction effect

1. Introduction

Liquid-crystal-on-silicon (LCOS) devices have great potential for microdisplay applications.^{1,2)} Because of the high electron mobility of silicon wafers, the pixel pitch of a high-resolution LCOS device can be made as small as 5–8 μm. Therefore, the light scattering and diffraction effects become significant and should be taken into account in the optical simulations. The conventional matrix-type methods^{3–5)} are based on the assumption of a stratified medium, for which the diffraction effect is intrinsically ignored. They are reliable only in the regime where the liquid crystal profiles are maintained uniformly over a scale far exceeding the optical wavelength, *e.g.*, in direct-view displays.

To analyze LCOS devices, the beam propagation method (BPM) has been proven useful.^{6,7)} This method is a numerical approach to the solution of Maxwell's curl equations. Unlike the matrix-type methods, the BPM considers the scattering and diffraction effects during the light propagation. Furthermore, its computational efficiency is much higher than that of the sophisticated finite-difference time domain (FDTD) method^{8–10)} and their results are almost identical when the liquid crystal (LC) layer is illuminated within ±30°. Although BPM has been employed for the calculations of the twisted nematic microdisplay,⁷⁾ the calculations were only focused on the transmissive-type devices. So far, this powerful tool has not been applied to analyzing the reflective-type display devices. Therefore, we extend the BPM to the reflective LCOS devices by using the

mirror-image concept.^{11,12)} Basically, the simulation consists of two parts: First, the LC director orientation is determined using a commercial software package, *2dimMos*, from Autronics. Second, the optical performance is calculated by the extended BPM with the finite difference algorithm.

In this work, two promising LC modes for LCOS applications, the high-contrast vertically aligned (VA)¹³⁾ mode and the fringing-field-less finger-on-plane (FOP)¹⁴⁾ mode, are studied. Simulation results are compared with those obtained using the Jones matrix method,³⁾ where the diffraction effect is ignored. A marked difference is observed. Moreover, we show that the optimization of the LCOS panels can be accurately carried out when the complex optical behaviors are clearly described. In §2, we introduce the mathematical method of the extended BPM and the parameters we used for simulations. In §3, the investigation of the optical behaviors of the VA and FOP modes are detailed.

2. Extended Beam Propagation Method for Reflective Liquid Crystal Displays

The beam propagation method starts with the solving of the following discretized Maxwell's curl equations:

$$\nabla \times H = j\omega\epsilon^*E \quad (1)$$

$$\nabla \times E = j\omega\mu_0H. \quad (2)$$

Here, ω is the angular frequency, μ_0 is the permeability of vacuum, and ϵ^* is the nine-element dielectric tensor given below:

$$\epsilon^* = \epsilon_0 \begin{bmatrix} n_o^2 + \Delta\epsilon_r \cos^2\theta \cos^2\phi & \Delta\epsilon_r \cos^2\theta \sin\phi \cos\phi & \Delta\epsilon_r \sin\theta \cos\theta \sin\phi \\ \Delta\epsilon_r \cos^2\theta \sin\phi \cos\phi & n_o^2 + \Delta\epsilon_r \cos^2\theta \cos^2\phi & \Delta\epsilon_r \sin\theta \cos\theta \cos\phi \\ \Delta\epsilon_r \sin\theta \cos\theta \cos\phi & \Delta\epsilon_r \sin\theta \cos\theta \sin\phi & n_o^2 + \Delta\epsilon_r \sin^2\theta \end{bmatrix} \quad (3)$$

$$\Delta\epsilon_r = n_e^2 - n_o^2,$$

where θ is the tilt angle and ϕ is the twist angle of the LC director. The angle definitions are illustrated in Fig. 1. The light waves are assumed to propagate in a nonmagnetic medium with the form of a harmonic time variation, *i.e.*, $\exp(j\omega t)$. The Crank-Nicolson scheme⁶⁾ is introduced to solve the differential eqs. (1) and (2) simultaneously. In order to prevent artificial reflections from the boundary,

transparent boundary condition (TBC)¹⁵⁾ is utilized to ensure that the outgoing radiation passes through the boundary freely. Finally, we can obtain the following sparse linear system:⁵⁾

$$\begin{bmatrix} [M_{11}(\theta, \phi)] & [M_{12}(\theta, \phi)] \\ [M_{21}(\theta, \phi)] & [M_{22}(\theta, \phi)] \end{bmatrix} \begin{bmatrix} [E_y^{s-1}] \\ [H_y^{s-1}] \end{bmatrix} = \begin{bmatrix} [C_1(E_y^s, H_y^s)] \\ [C_2(E_y^s, H_y^s)] \end{bmatrix}. \quad (4)$$

*E-mail address: simonf.eo89g@nctu.edu.tw

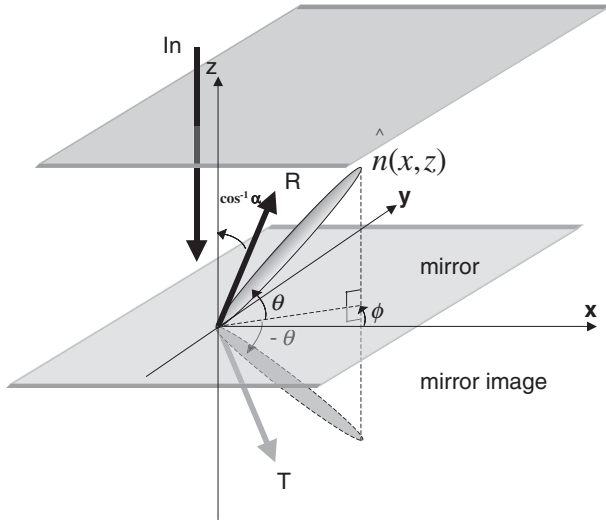


Fig. 1. Schematic representation of angle definitions and mirror image of reflective LCOS device.

Each of the sub-blocks $[M_{i,j}]$ with $i, j = 1, 2$ corresponds to a tridiagonal matrix. Superscript $s = 1, 2, \dots, n$ indicates the propagation step of the discretized axial plane, i.e., $z = s\Delta z$ assuming that z is the propagation direction of the light. E_y and H_y are the electric and magnetic fields in the y direction, respectively. Both C_1 and C_2 are functions related to E_y^s and H_y^s . By solving eq. (4) with an initial condition of a plane wave propagating along the z direction, we can obtain information that includes the amplitude and phase of the propagating light wave.

The reflective propagation process of the light wave can be derived by sending the light into the mirror image of the LC molecular distribution, as shown in Fig. 1. Therefore, the reflective transverse fields, E_{ry} and H_{ry} , of the LCOS device can be described as follows:

$$\begin{aligned} E_{ry}^1 &= R_{g,p} \times E_y^n \\ H_{ry}^1 &= R_{g,p} \times H_y^n \end{aligned}$$

$$\begin{aligned} \begin{bmatrix} [M_{11}(-\theta, \phi)] & [M_{12}(-\theta, \phi)] \\ [M_{21}(-\theta, \phi)] & [M_{22}(-\theta, \phi)] \end{bmatrix} \begin{bmatrix} [E_{ry}^{s+1}] \\ [H_{ry}^{s+1}] \end{bmatrix} \\ = \begin{bmatrix} [I_3(E_{ry}^s, H_{ry}^s)] \\ [I_4(E_{ry}^s, H_{ry}^s)] \end{bmatrix}, \end{aligned} \quad (5)$$

where R_p and R_g represent the reflectance of the reflective pixels and the interpixel gap, respectively. From eq. (1), we obtain

$$-\frac{\partial H_{ry}}{\partial z} = j\omega\epsilon_0(\epsilon_{xx}E_{rx} + \epsilon_{xy}E_{ry} + \epsilon_{xz}E_{rz}) \quad (6a)$$

$$\frac{\partial H_{ry}}{\partial x} = j\omega\epsilon_0(\epsilon_{zx}E_{rx} + \epsilon_{zy}E_{ry} + \epsilon_{zz}E_{rz}). \quad (6b)$$

The reflected fields polarized in the x and z directions (i.e., E_{rx} and E_{rz}) can be derived from eqs. (6a) and (6b):

$$E_{rx} = -\frac{1}{j\omega\epsilon_0\zeta} \left(\epsilon_{zz}^* \frac{\partial H_{ry}}{\partial z} + \epsilon_{xz}^* \frac{\partial H_{ry}}{\partial x} \right) - \frac{\xi}{\zeta} E_{ry} \quad (7a)$$

$$E_{rz} = \frac{1}{j\omega\epsilon_0\zeta} \left(\epsilon_{xx}^* \frac{\partial H_{ry}}{\partial x} + \epsilon_{zx}^* \frac{\partial H_{ry}}{\partial z} \right) - \frac{\zeta}{\zeta} E_{ry}, \quad (7b)$$

where

$$\begin{aligned} \zeta &= \epsilon_{xx}^* \epsilon_{zz}^* - \epsilon_{zx}^* \epsilon_{xz}^*, & \zeta &= \epsilon_{xx}^* \epsilon_{zy}^* - \epsilon_{zx}^* \epsilon_{xy}^*, \\ \xi &= \epsilon_{xy}^* \epsilon_{zz}^* - \epsilon_{zy}^* \epsilon_{xz}^*. \end{aligned}$$

After we have obtained the information concerning the propagating fields, it is important to further investigate the angular distribution of the light intensity, which is called the intensity angular spectrum. By using Fourier transform, the amplitude angular spectra, $A_{x,y}(\alpha/\lambda)$, of the transverse fields, E_{rx}^n and E_{ry}^n , are given as follows:

$$A_{x,y} \left(\frac{\alpha}{\lambda} \right) = \int E_{rx,ry}^n \exp \left[j2\pi \left(\frac{\pi/2 - \alpha}{\lambda} x \right) \right] dx, \quad (8)$$

where λ is the light wavelength in the propagation medium and α represents the cosine of the beam propagation direction depicted in Fig. 1. Finally, the output intensity angular spectrum is expressed as:

$$I \left(\frac{\alpha}{\lambda} \right) = A_x^2 + A_y^2. \quad (9)$$

Equation (7) represents the spectrum of the light at the end of the propagation prior to entering the cover glass. When considering the spectrum of the light exiting the LC panel, the refractions at the interfaces of the cover glass and the air must be taken into consideration. As a consequence, the final propagation angle, θ_p , is given as follows:

$$\theta_p = \sin^{-1}(n_{\text{eff}}^n \times \sin(\cos^{-1} \alpha)), \quad (10)$$

where n_{eff}^n represents the effective refractive index at the end of the propagation in the LC layer. We then define the light efficiency of the LCOS panels, η , as follows:

$$\eta = \frac{\int_{-\theta_a}^{\theta_a} I \left(\frac{\theta_p}{\lambda} \right)}{I_{\text{in}}}, \quad (11)$$

where I_{in} is the intensity of the incident light and θ_a represents the acceptance angle of the optical system which is related to the f-number ($F_{\#}$) of the system:

$$\theta_a = \tan^{-1} \left(\frac{1}{2F_{\#}} \right). \quad (12)$$

Figure 2 shows the cell structures used for the two-dimensional (2D) simulations of the LC director distributions and light efficiencies. The value of $d\Delta n$ equals 207.5 nm for the FOP mode and 190.9 nm for the VA mode, where d is the cell gap and Δn is the LC birefringence. The LC parameters used for simulations are based on the commercial material MLC-6608 and are listed in Table I.

Table I. LC parameters used in simulations.

Simulation Parameter	Value
Splay elastic constant, K_{11}	16.7×10^{-12} N
Twist elastic constant, K_{22}	7×10^{-12} N
Bend elastic constant, K_{33}	18.1×10^{-12} N
Static dielectric constant (parallel), ϵ_{\parallel}	3.6
Static dielectric constant (perpendicular), ϵ_{\perp}	7.8
Ordinary refractive index, n_o	1.4748
Extraordinary refractive index, n_e	1.5578

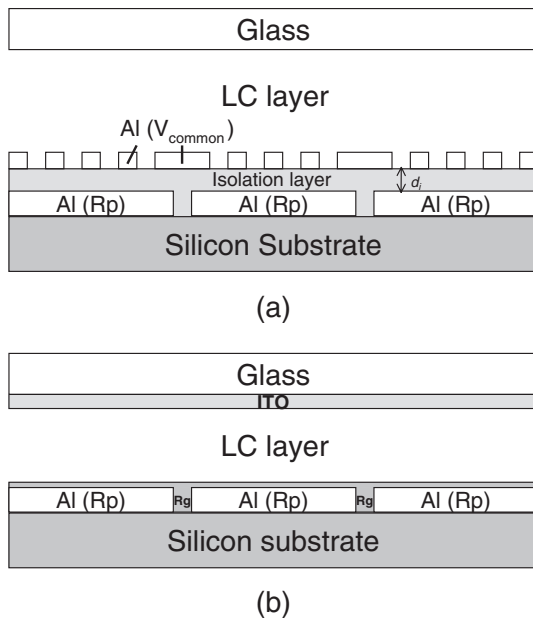


Fig. 2. Cell structures used for 2D computer simulations of (a) FOP mode (b) VA mode.

The LCOS panels are both illuminated by normally incident linearly polarized light. The angles between the polarization direction and the LC rubbing direction on the top glass are 0° and 45° for the FOP mode and the VA mode, respectively. In our optical engine, we assume $F_\# = 2.8$, which indicates $\theta_a \sim 10^\circ$. In order to investigate the influence of the pixel pitch (P) on the light efficiency, we varied the P/λ value in the range from 30 to 2.5 with a fixed interpixel gap ($0.7 \mu\text{m}$). The LC layer is divided into a grid with the spatial step

$\Delta x = 100 \text{ nm}$ and $\Delta z = 50 \text{ nm}$ during the numerical analyses. In simulations, we assume $R_p = 90\%$ and $R_g = 0\%$ for the pixilated aluminum electrodes and absorptive black matrices underneath the interpixel regions, respectively.

3. Diffraction Effects on FOP- and VA-LCOS Devices

Figures 3(a) and 3(b) plot the calculated light efficiencies ($\theta_a = 10^\circ$) of the LCOS devices with respect to the P/λ value when all the pixels are turned off for the FOP and VA modes, respectively. The results calculated by the Jones matrix method are also included in the figures. From Fig. 3(a), the light efficiencies predicted by the BPM are much lower than those given by the Jones matrix method. In reality, the comb-like common electrodes on the bottom substrate of the FOP device act as a phase grating. The light waves encountering these electrodes are scattered and diffracted at various angles. The light waves propagating outside the acceptance angle of the projection lens are wasted. Thus, the overall light efficiency is decreased. It is well known from the grating formula that $m\lambda = a \sin \theta$ (where m is the order of diffraction, a is the grating pitch and θ is the diffraction angle); thus, the diffraction angle gets larger as the pitch becomes smaller. Therefore, a smaller pixel pitch generally gives a lower light efficiency in LCOS devices. However, some exceptions may occur. For example, when $P/\lambda = 5$ in Fig. 3(a), the diffraction angle of the first-order light exceeds the critical angle of the total internal reflection at the glass-air interface so that the energy cannot escape from the device. As a result, the light efficiency is higher than that of the condition with a larger P/λ .

We have shown that the BPM describes the optical behavior of the FOP device reasonably well. The Jones matrix results are almost identical for different pixel pitches

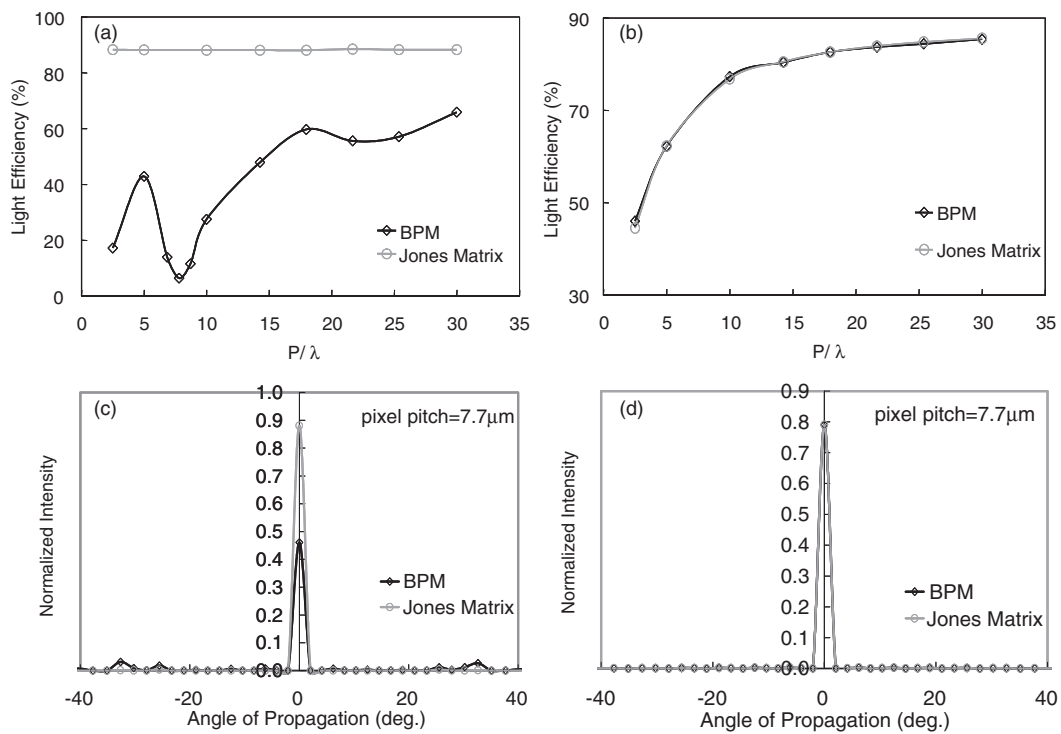


Fig. 3. Computer simulated results of LCOS devices in voltage-off state by extended BPM and Jones matrix method: light efficiencies ($\theta_a = 10^\circ$) of LCOS devices with respect to P/λ value for (a) FOP mode; and (b) VA mode, and intensity angular spectrum with $P = 7.7 \mu\text{m}$ and $\lambda = 540 \text{ nm}$ for (c) FOP mode; and (d) VA mode.

and are much higher than those obtained by the BPM. Basically, the Jones matrix method treats the bottom substrate only as a specular reflector. Figure 3(c) shows the intensity angular spectrum calculated by both methods with $P = 7.7 \mu\text{m}$ and $\lambda = 540 \text{ nm}$. It can be easily seen that without consideration of the diffraction effect, the signal light waves mainly propagate along the normal direction, which would cause an unbearable error in a real system.

In the VA mode, an absorption material (black matrix) is imbedded underneath the interpixel gaps. In the voltage-off state, the device acts as a slit grating. The calculated light efficiencies from the BPM and the Jones matrix method are almost the same, as shown in Figs. 3(b) and 3(d). However, the voltages between the adjacent pixels are different when an image is displayed. Therefore, we simulated the extreme case in which one pixel is on and its adjacent pixels are off, i.e., the off-on-off configuration.

Figure 4(a) shows the calculated light efficiencies of the

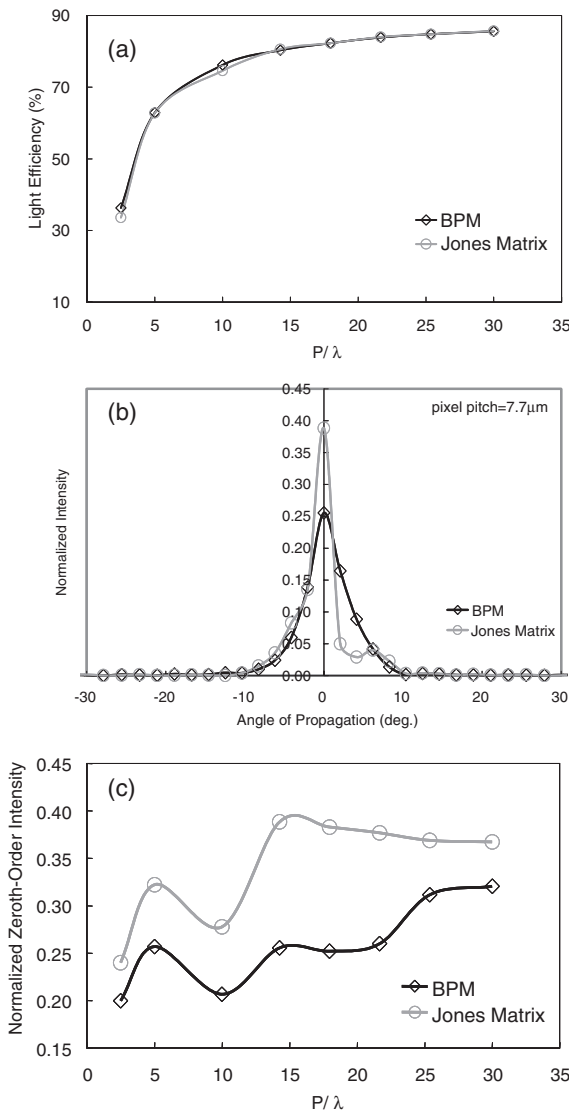


Fig. 4. Computer simulated results of VA mode with off-on-off pixel configuration by extended BPM and Jones matrix method: (a) light efficiencies ($\theta_a = 10^\circ$) of LCOS devices with respect to P/λ value, (b) intensity angular spectrum with $P = 7.7 \mu\text{m}$ and $\lambda = 540 \text{ nm}$, and (c) the intensity of zeroth-order diffracted light, I_0 , calculated with respect to P/λ value.

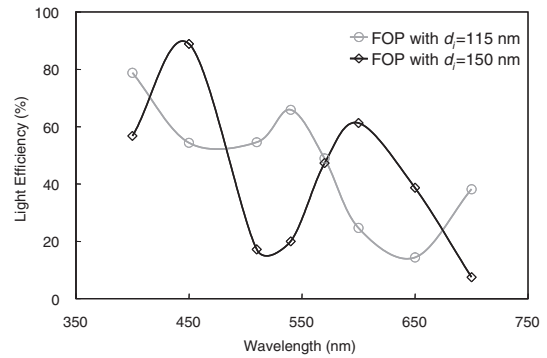


Fig. 5. Calculated light efficiency by reflective BPM with respect to wavelength for FOP mode ($P = 15.5 \mu\text{m}$) with $d_i = 115 \text{ nm}$ and 150 nm .

VA device as functions of P/λ . Although this figure still shows almost identical results for the two methods, the optical behaviors are very different. Figure 4(b) shows the calculated intensity angular spectra with $P = 7.7 \mu\text{m}$ and $\lambda = 540 \text{ nm}$. As shown in the figure, the intensities of the signal light near the normal direction calculated by the BPM are much lower than those calculated by the Jones matrix method. The intensity of the zeroth-order diffracted light, I_0 , is also calculated with respect to the P/λ value, as shown in Fig. 4(c). The I_0 calculated by the BPM is always lower due to the light scattering and diffraction by the various LC orientations around the pixel edges. These results are particularly important for designing a projection display, because accurately predicting the angular distribution of the light intensity can prevent many unwanted image aberrations in the optical system.

This extended BPM simulator is useful for designing high-resolution LCOS devices. For example, we simulated the light efficiency with respect to the wavelength for the FOP mode ($P = 15.5 \mu\text{m}$) for different values of d_i , as shown in Fig. 5. From the figure, the green (G) band exhibits a higher efficiency at $d_i = 115 \text{ nm}$ while the red (R) and blue (B) bands favor $d_i = 150 \text{ nm}$. Therefore, one can boost the efficiency of the FOP device in a two- or three-panel projection system by optimizing the value of d_i corresponding to the R, G and B bands, respectively. In order to do this, a good simulation tool, such as the BPM, is needed to optimize the value of d_i as well as other parameters. It is noteworthy mentioning that the simulated results with $d_i = 115 \text{ nm}$ in Fig. 5 have similar trend to the experimental results published by Chou *et al.*¹⁴⁾

4. Conclusions

The conventional matrix-type methods cannot authentically simulate the optical characteristics of LCOS devices as the pixel pitch is comparable to the wavelength. We extend the BPM to calculate the optical performance of the high-resolution LCOS devices. Light scattering and diffraction effects are included in the simulations. Two promising LC modes: vertically aligned and finger-on-plane LCOS devices are analyzed. Our results indicate that both modes are significantly influenced by the diffraction effect. The calculated light efficiency strongly depends on the pixel pitch. The optical behaviors are also explicitly described from the intensity angular spectra. We have shown that it is essential to employ the BPM for designing LCOS devices.

Acknowledgements

This work was partially supported by the National Science Council, R.O.C., under the Contract No. NSC 93-2112-M-009-022.

- 1) P. M. Alt: Conference record of the Int. Display Research Conf. M19-28 (1997).
- 2) H. Kurogane, K. Doi, T. Nishihata, A. Honma, M. Furuya, S. Nakagaki and I. Takanashi: Soc. Inf. Display Tech. Dig. **29** (1998) 33.
- 3) R. C. Jones: J. Opt. Soc. Am. **31** (1941) 488.
- 4) D. W. Berreman: J. Opt. Soc. Am. **62** (1972) 502.
- 5) A. Lien: Appl. Phys. Lett. **57** (1990) 2767.
- 6) E. E. Kriezis and S. J. Elston: J. Mod. Opt. **46** (1999) 1201.
- 7) E. E. Kriezis and S. J. Elston: Appl. Opt. **39** (2000) 5707.
- 8) B. Witzigmann, P. Regli and W. Fichtner: J. Opt. Soc. Am. A **15** (1998) 753.
- 9) E. E. Kriezis and S. J. Elston: Opt. Commun. **165** (1999) 99.
- 10) E. E. Kriezis and S. J. Elston: Opt. Commun. **177** (2000) 69.
- 11) C. L. Kuo, C. K. Wei, S. T. Wu and C. S. Wu: Jpn. J. Appl. Phys. **36** (1997) 1077.
- 12) S. T. Wu and D. K. Yang: *Reflective Liquid Crystal Displays* (Wiley, New York, 2001).
- 13) M. F. Schiekol and K. Fahrewnschon: Appl. Phys. Lett. **19** (1971) 391.
- 14) W. Y. Chou, C. H. Hsu, S. W. Chang, H. C. Chiang and T. Y. Ho: Jpn. J. Appl. Phys. **41** (2002) 7386.
- 15) G. R. Hadley: IEEE J. Quantum Electron. **28** (1992) 363.